Published in final edited form as:
Acta Biomater. 2012 December ; 8(12): 4334–4341. doi:10.1016/j.actbio.2012.07.007.

Microbubbles as Biocompatible Porogens for Hydrogel Scaffolds

Eric G. Lima[1], **Krista M. Durney**[1], **Shashank R. Sirsi**[2], **Adam B. Nover**[3], **Gerard A. Ateshian**[3,4], **Mark A. Borden**[2], and **Clark T Hung**[3,*]

[1]The Cooper Union, New York, NY, 10003, USA

[2]Department of Mechanical Engineering, University of Colorado at Boulder, Boulder, CO, 80309, USA

[3]Department of Biomedical Engineering, Columbia University, New York, NY, 10027, USA

[4]Department of Mechanical Engineering Columbia University, New York, NY, 10027, USA

Abstract

In this study, we explored the application of lipid-shelled, gas-filled microbubbles as a method for creating on-demand microporous hydrogels for cartilage tissue engineering. The technique allowed for homogenous distribution of cells and micropores within the scaffold, increasing the absorption coefficient of large solutes (70 kDa dextran) over controls in a concentration-dependent manner. The stability of the gas-phase of the microbubbles depended on several factors, including the initial size distribution of the microbubble suspension, as well as the temperature and pressure during culture. Application of pressure cycles provided controlled release of the gas phase to generate fluid-filled micropores with remnant lipid. The resulting microporous agarose scaffolds were biocompatible, leading to a 2-fold increase in engineered cartilage properties (EY=492 ± 42 kPa for bubble group vs. 249 ± 49 kPa for bubble-free control group) over a 42-day culture period. Our results suggest that microbubbles offer a simple and robust method of modulating mass transfer in cell-seeded hydrogels through mild pressurization, and the methodology may be expanded in the future to include focused ultrasound for improved spatio-temporal control.

Keywords

cartilage tissue engineering; size-isolated microbubbles; triggered gas dissolution; hydrostatic pressure; articular chondrocytes

1. Introduction

Designing biocompatible scaffolds with architecture that optimizes solute transport is challenging for fields such as cartilage tissue engineering. If scaffold architecture is too dense, nutrient supply becomes insufficient and cells die or underperform [1]. However, if scaffold porosity is too high, cell products are lost to the bathing culture medium to the

*Corresponding Author: Clark T. Hung, Professor of Biomedical Engineering, 351 Engineering Terrace, 1210 Amsterdam Avenue, Mail Code: 8904, Phone: +1 212-854-6542 Fax: +1 212-854-8725, cth6@columbia.edu.

detriment of tissue development. An ideal tissue scaffold would provide a balance between a local pore structure sufficient to retain cell products that form extracellular matrix (ECM) tissue and a global architecture that provides adequate nutrient supply to cells at the central core regions of the scaffold. This is a difficult challenge because the cross-sectional thickness of cartilage varies considerably across the human joint (ranging from 1-6 mm across the patella), so engineers must design scaffolds that optimize solute transport across a wide range of diffusion distances. Secondly, the scaffold architecture itself is transformed with culture time by cell-mediated synthesis of ECM, so the diffusivity of some important solutes (such as growth factors) is reduced over time. In short, the spatio-temporal development of these nutrient gradients must be accounted for when designing scaffolds for larger construct applications.

Agarose has been used extensively in cartilage biology [2-5]. and is currently being evaluated in human clinical trials as a scaffold component of a next generation autologous chondrocyte implantation strategy [6, 7]. We have found that 2% agarose (Type VII, Sigma) permits robust cartilaginous tissue growth with Young's moduli (E_Y) and glycosaminoglycan (GAG) levels similar to that of native tissue after ≤8 weeks in culture [8]. This robust growth, however, is limited to small cylindrical constructs. We have observed that constructs of >1 mm thickness develop a “U-shaped” axial distribution of properties beginning at ~2 weeks with central regions having less matrix elaboration relative to stiffer peripheral regions [9]. The development of inhomogeneous tissue properties with culture time is presumably due to nutrient limitations at the core region. From Fick's law, the diffusion time of a solute is proportional to the square of the distance (Distance^2 Diffusivity × Time), so even small changes in scaffold thickness can have major impacts on tissue growth.

As with most hydrogels, the pore size of agarose decreases with polymer concentration [1]. Researchers are therefore examining methods to increase nutrient availability while maintaining the polymer concentration and local pore size (~Ø232 nm) [1]. that was found to be effective in the development of small engineered constructs (volume: 0.0126 mL). Recently, we obtained successful results while doubling the volume of the constructs (0.0288 mL) by the use of embedded channels of 0.5-1 mm diameter into the newly formed gel to provide solute exchange [9]. The channels in these gels slowly closed over time, so the initial diameter of the channel and the channel spacing needed to be carefully controlled. In the current study, we aim to complement this strategy through the use of microbubbles as a porogen for agarose hydrogels. The porogen can be spatially and temporally controlled to fine-tune nutrient exchange within the construct while balancing entrapment of cell synthesized matrix products.

Microporosity in bioscaffolds is typically formed using sacrificial porogens that are dissolved away using cell-incompatible techniques. For example, pores have been made by water-in-oil emulsification using solid granules of calcium carbonate [10], and metal oxides have also been used for poration within agarose gels [11]. Similarly, lyophilization of hydrogels can result in sponge-like scaffolds with microporosity, but again the lyophilization process is not biocompatible [12, 13]. For these systems, cells are introduced via seeding techniques that depend on the effectiveness of cell infiltration to central regions of the construct to achieve uniform seeding. Unlike hydrogels, pore sizes in these constructs are constrained to a minimum diameter that allows for cell infiltration. The microbubble encapsulation process described here enables the direct *ab initio* immobilization of cells within gels that have a homogenous micropore distribution. Few fabrication processes permit such direct cell immobilization, which has the benefit of allowing the local hydrogel pore size to be smaller than the cell diameter.

We anticipate that modulating the microporosity of agarose hydrogels by using controlled dissolution of microbubbles will allow for more effective nutrient transport to embedded cells and thereby increase tissue properties over time. Our specific hypothesis is that cell-seeded, microbubble-encapsulated hydrogel scaffolds will yield engineered cartilage with more native cartilage properties compared to cell-seeded, microbubble-free hydrogel constructs.

2. Materials and Methods

2.1 Experimental Design

Two studies were carried out: *Characterization of acellular constructs* examined the concentration-dependent changes in mechanical properties and solute uptake rates in acellular microbubble constructs. Additionally, we examined the persistence of microbubbles within the gel over culture time compared to a forced dissipation of the bubbles using applied hydrostatic pressure. *Characterization of cell-seeded constructs* examined the biocompatibility of cell-seeded microbubble constructs by tracking the deposition of cell products along with changes in mechanical properties through culture time.

2.1.1. Characterization of Acellular Constructs—Sterile microbubbles were created through sonication of 90% distearoylphosphatidylcholine (DSPC) and 10% polyoxyethylene-40 stearate (PEG40S) lipid solution in the presence of a small perfluorobutane (PFB) gas headspace [14]. The resulting bubble mixture was counted and sized (~1-10 um) using an Accusizer 780A (Particle Sizing Systems, Santa Barbara, CA) [14]. to determine total gas volume. When applicable, microbubbles were size-isolated using a differential centrifugation technique described previously [14, 15]. to achieve microbubble suspensions with diameters ranging from 4-5 um.

To create microbubble constructs, one volume of low-melt agarose (Type VII, Sigma) at 4% [g/ml of phosphate buffered saline (PBS)]. was mixed with an equal volume of microbubble suspension to generate final microbubble concentrations. Concentrations were chosen based on the percentage of agarose volume that was displaced by inclusion of microbubbles (0.0%, 0.5%, 1.0%, 2.0%).

2.1.2. Characterization of Cell-Seeded Constructs—Articular chondrocytes were enzymatically harvested from bovine carpo-metacarpal joints from freshly slaughtered 4-6 month old calves obtained from a local abattoir [16]. Cells were typically combined from wrist joints of 3-4 animals. A microbubble cell suspension was then created by combining the cells and bubbles directly. This suspension was added to agarose as in the previous study with acellular constructs and gelled in sterile molds to yield a final cell concentration of 30×10^6 cells/ml in 2% w/v agarose with a volume concentration of 0.5% and 2.0% microbubbles. Disks of 4 mm diameter were cored out using a biopsy punch. Constructs were maintained in culture for up to 42 days, with three-times weekly changes of chondrogenic growth medium (with 5 g/mL proline, 1% ITS+ (BD Biosciences- insulin, human transferrin, and selenous acid), 100 nM dexamethasone, 50 μg/mL ascorbate, and 10 ng/mL of TGF- 3) for the first 2 weeks [8, 17]. Since microbubble-infused constructs tended to float, exposing some surfaces to air, a small polymer mesh (PTFE Diamond Mesh 0.080″ × 0.025″, www.McMaster.com) was placed on top of the constructs to keep them submerged.

2.2 Triggered Gas Dissolution

Microbubbles embedded in the agarose scaffold were purged of gas through the application of hydrostatic pressure (~289 kPa) by compressing a fluid-filled syringe in a mechanical testing apparatus (Instron, Norwood, MA) with known displacement and force (Figure 2). The efficiency of gas removal was quantified by the difference in wet weight before and after the application of hydrostatic pressure. To obtain the wet weight post-pressure, constructs were removed from the syringe and briefly blotted on paper towels to remove excess fluid. Control disks were subjected to the same experimental setup to account for any effects of the transient applied pressure, which is more than an order of magnitude lower than physiologic pressures during joint loading [18].

2.3. Assessment of Construct Properties

The absorption coefficient was determined by maintaining constructs in a bathyof fluorescein isothiocyanate (FITC)-conjugated dextran (70 kDa, Molecular Probes, NY) and measuring the ratio of the concentration of dextran captured inside the disk to that of the bathing solution, as previously described [19, 20]. Local diffusion was then analyzed within the constructs using fluorescence recovery after photobleaching (FRAP) on a confocal microscope (Fluoview FV1000, Olympus). Following FRAP, constructs were placed in the incubator (37°C) for one week to facilitate microbubble dissolution, after which the FRAP procedure was repeated. FRAP images were processed and analyzed using custom MATLAB codes to yield an average diffusivity coefficient, D, for each group [21].

For cell-seeded constructs, mechanical properties (Young's Modulus, E_Y and Dynamic Modulus at 0.5 Hz, G*) were assessed via a custom testing device [16]. Briefly, constructs were subjected to a stress relaxation test to 10% strain in a PBS bath in unconfined compression between two impermeable platens. Once equilibrium was reached, a dynamic compression test was conducted at 0.5 Hz and 2% strain. Constructs were then cut in half and saved for either biochemical assays or fixed for histological analysis. Biochemical assessment included glycosaminoglycans (GAG) using the 1,9-dimethylmethylene blue assay, collagen using the hydroxyproline assay, and DNA content using the picogreen assay, along with histology (safranin-O for GAG distribution, picrosirius red for collagen distribution) as described previously [9, 22, 23]. Biochemical data was normalized to wet weight for each construct.

2.4. Statistical Analyses

Post-hoc analyses were done using ANOVA with Tukey's post hoc test using Statistica (StatSoft, OK). Each study was repeated at least twice and, in the cellular study, using cells from independent cell preparations. Sample sizes ranged from 5-6 samples per iteration, with results pooled across repeat studies for a total of 10-12.

3. Results

Figure 1A shows a schematic of the assembly protocol where microbubbles were mixed homogenously with a cell suspension and then combined to form the final cell-seeded microbubble hydrogel constructs. Casting did not require any special equipment beyond that which is required for producing control gels (mold, sterile hood, etc). Figure 1B shows the expected solute path between control gels and microbubble gels, both before and after the gas inside the microbubbles was purged.

Figure 2A shows the gross morphology of the resulting microbubble constructs with a concentration-dependent opacity. Higher microbubble concentrations resulted in more

opaque constructs. At concentrations above 0.5% v/v, constructs began to float in PBS or in culture media (Figure 2B).

Figure 2C shows the application of hydrostatic pressure. Constructs alternatively sunk and then floated again with each cycle of pressure. However, over 3 hours of loading, these constructs began to lose some of their buoyancy, eventually settling on the bottom of the syringe. Figure 2D shows the gross appearance of microbubble constructs at various times through hydrostatic pressure loading period, clearly depicting the loss of opacity from the periphery towards the core of the constructs over time. Figure 2E shows the density before and after the cyclic application of hydrostatic pressure. The density of the 2.0% v/v microbubble group was initially significantly lower than the 0.0% v/v (control) group, but after 3 hours of cyclic loading, the densities were equal. There is an increasing, but statistically non-significant, trend in the densities of all constructs after the application of pressure, but we believe this is an artifact of the testing process where excess fluid from the bathing medium clung to the constructs during weighing.

In an initial set of acellular studies we found that microbubbles would coarsen over time (Day 14) into large macrobubbles (~1-2mm in diameter). These initial studies were carried out using microbubbles that had not been size-isolated prior to casting in agarose (ranging from 1-10μm in diameter). Size-isolation of microbubbles to a narrower range (~4 μm in diameter) seemed to eliminate the appearance of these macrobubbles, as they did not occur in any subsequent study.

Figure 3A shows a microscopic view of the microbubbles in PBS; the spherical shape and homogenous size distribution is clearly evident. Figure 3B is a graph showing the size distribution of microbubbles as measure on an acusizier device. The number of microbubbles is binned in terms of microbubble diameter. The mean and median diameter is also expressed.

Figure 4a shows a microscopic view (20×) of 2.0% v/v microbubble constructs that have been soaked in a solution of FITC-labeled 70 kDa dextran on day 1 of the experiment. Black regions show the exclusion of dextran due to the presence of gas-filled microbubbles. The microbubbles were homogenously distributed throughout the gel. Micropores within the gel ranged from 1-10μm in diameter and were not interconnected. Figure 4b shows the same set of constructs after 7 days of free-swelling culture (day 8), where the majority of black regions have been replaced with regions of bright green. These regions had the same fluorescent intensity as the bathing media of saturated FITC-dextran (data not shown). Visual inspection of the whole constructs showed that they became transparent. Figure 4C shows the control samples (0.0% v/v microbubbles on day 8). For comparison of dissolution rates, a set of free-floating microbubbles (i.e. not encapsulated in agarose) was maintained in a sterile petri dish with PBS in both the incubator and the refrigerator. These bubbles decreased in number from 2.0×10^9 initially to 1.3×10^8 (at 4°C) or 4.7×10^7 (at 37°C) in 96 hours (data not shown).

Figure 4D and 4E show the lipid microbubbles visualized as red with the lipophilic tracer (Dil) in 2.0% v/v constructs on day 8. The pools of green FITC-conjugated dextran and the red lipid tracer dye are co-localized, suggesting that the lipid layer remains in place after the gas-phase dissolves away.

Figure 5A shows the absorption coefficient (defined as the concentration of dextran in the construct normalized by the concentration of dextran in the bathing solution) as a function of microbubble concentration. After 3 hours of exposure, the absorption coefficient was significantly higher in microbubble constructs in a concentration-dependent manner, with the highest absorption-coefficient in the 2.0% v/v group.

Figure 5B shows the absorption coefficient as a function of time (rather than microbubble concentration as in Figure 5A). In this case, 2.0% v/v microbubble constructs were compared against 0.0% v/v control constructs, with significant differences between absorption coefficients observed at 6 and 9 hours.

Figure 5C shows the diffusion coefficients ($\mu m^2/s$) determined by FRAP analysis of 70 kDa dextran through 2.0% v/v microbubble constructs on day 1 and on day 8 compared to 0.0 % v/v control gels. Interestingly, the diffusion coefficient through microbubble gels was initially significantly lower than for bubble-free controls, but by day 8 this difference was no longer significant.

Figure 6A) shows bright field microscopy images of a 2.0% v/v microbubble infused cellular constructs where microbubbles (but not cells) are clearly visible. Figure 6B) shows fluorescence microscopy of the same construct where the Calcein AM dye highlights living cells (but not bubbles) in fluorescent green. Figure 6C) shows simultaneous visualization of cells and bubbles.

Figure 7 top) shows the Young's Modulus of cell-seeded microbubble constructs (0.0% v/v, 0.5% v/v, and 2.0% v/v) over culture time with significantly higher values for the 2.0% v/v microbubble group after 42 days in culture. Although not apparent due to the scale of the graph, the Young's modulus of constructs immediately after casting were significantly different from each other (0.0% control = 15 ± 4 kPa; 0.5% μb = 9 ± 3 kPa; 2.0% μb = 6 ± 2 kPa).

Figure 7 Bottom) shows a chart of other relevant mechanical and biochemical properties, including a significant increase in the dynamic modulus (G* at 1 Hz) for the 2.0% v/v group, as well as significant increases in GAG/DNA and collagen/DNA. There were no quantifiable differences in GAG or collagen distributions evident from histological staining (not shown).

4. Discussion

In this study, we explored the application of lipid-shelled, gas-filled microbubbles [24-26]. as a method for creating cell-laden microporous hydrogels for cartilage tissue engineering. Our data demonstrates a 2-fold increase in engineered cartilage properties in hydrogels with microbubble-derived microporosity (Figure 7), an effect of greater proportion than observed previously with applied deformational loading [27]. As such, we believe that this is a promising approach towards creating engineered cartilage with more native cartilage properties.

Our strategy is similar in principle to that recently described for agarose hydrogels using sucrose porogens (that dissolve in culture media) [28]. In this system, solute diffusivity of the cell-laden hydrogel was shown to increase with sucrose porogen concentration. Microbubble porogens proposed herein achieve similar concentration-dependent results, but retain certain advantages over the sucrose system. Through the use of a highly dilute and biologically inert gas, microbubbles do not cause osmotic shock to cells that may pose a problem with the sucrose system.

The lipid monolayer shell is approximately 10 nm thick [29, 30]. and provides mechanical stability to resist growth and dissolution [31]. The lipid shell forms an effective gas barrier, preventing the development of a direct gas-liquid interface and preventing embolic, thrombogenic or immunogenic effects. Gas filled microbubbles can be mixed directly with cells and unpolymerized hydrogels (Figure 6). Over time two concurrent dissolution processes take place: 1) The gas species initially in the core diffuse away (since the lipid

shell has a permeability to oxygen of ~0.01 cm/s) and equilibrium is established between the gas core and species of gas in the surrounding aqueous environment [32, 33], and, 2) The bubbles themselves begin to collapse, leaving behind fluid-filled pores as they dissolve (Figure 4). Under the current culture conditions the bubbles remained persistent for up to a week in culture (Figure 4). Microbubbles can also be forced to dissolve on-demand by exposure to applied hydrostatic pressure or to focused ultrasound (Figure 2 and 3). The former would allow for temporal control of pore placement which may be an advantage in directing nutrient supply over time, while the latter may allow the triggering of microbubble dissolution in specific sub-regions of the whole construct [34], thereby allowing for both spatial and temporal control.

During dissolution, the lipid shell buckles and sheds into the aqueous surroundings to form small, fluid-filled lamellar vesicles [35-37], as supported by our data showing a drastic increase in density with the onset of pressurization (Figure 2) and visualized in Figures 3 and 4. Thus, compared to classical porogen techniques, microbubble dissolution can be triggered on demand.

Although the production of microbubble-infused hydrogels was uncomplicated; care must be taken to size-isolate the bubbles prior to casting to avoid a coarsening process where smaller microbubbles ripen to form larger macro-bubbles. Our data showed that bubbles of predominately 4 um were sufficient to prevent coarsening.

While microbubbles have been used for a decade as an FDA-approved intravascular contrast agent for echocardiography [38-40], recently microbubbles are being examined as a means for molecular imaging [41, 42]. and targeted drug-delivery [33, 43-45]. Nair et al incorporated large growth-factor laden albumin microbubbles (>50 um) into polymer tissue scaffolds [46], and Epstein-Barash et al. developed an ultrasonic cavitation model for drug-delivery using lipid-coated microbubbles and liposomes in agarose [33]. The potential to release chemical factors (e.g., growth factors, drugs, plasmids) tethered to the microbubbles during triggered dissolution represents a unique on-demand delivery method (coincident with micropore formation) not possible with other microporosity formation strategies for hydrogels [24, 25, 33]. Intriguingly, a microbubble formulation that was stable under hydrostatic pressure for longer periods of time may allow for the platenless deformation of microbubble-infused hydrogel constructs. In such a scenario, cyclic hydrostatic pressure or ultrasound would be used to compress and expand the gas phase of the microbubbles [47]. Thus, in addition to altering porosity and delivering growth factors, microbubble porogens may allow for deformation and convection within the hydrogel.

Our data shows an interesting contrast between the absorption coefficient, which increased with inclusion of microbubbles (Figure 5A, 5B), and the diffusion coefficient, which initially decreased with the inclusion of microbubbles (Figure 5C). The absorption coefficient is a measure of how much solute is retained in the construct over a period of time; whereas the diffusion coefficient is a measure of how rapidly solute moves through the constructs. Dissolution of microbubbles results in the creation of fluid-filled pores in the gel matrix. Co-localization of the lipophilic tracer dye and the fluorescently-labeled dextran suggest that the lipid shell at least partially remains in the pocket created by the microubble, even after the gas has been evacuated (Figure 4). The residual phospholipid particles constitute less than 3% of the volume for a 1-μm radius microbubble, and they are bioresorbable. Nonetheless, we were concerned that the remnants of the lipid shell would impede solute movement. Figure 5D indicates that the gas-filled microbubbles were initially obstacles to diffusion (as suggested in Figure 1). However, as the microbubbles dissolved over time, the diffusion coefficient increased to baseline (i.e., for the purely nanoporous

gel). The rate limiting step was therefore diffusion through the gel matrix, not the micropores or the remnants of the lipid shell.

Together, these findings suggest that the underlying mechanism governing the beneficial effects of microbubbles may be the ability of the pores they create to act as reservoirs of cell nutrients and chemical factors from within the engineered constructs during *in vitro* growth (Figure 4A, 4B). This differs from our original hypothesis (Figure 1A) that microbubbles would increase solute diffusivity through the gel by effectively decreasing the nutrient path length via the superposition of microporosity over the nanoporosity of the gel. In our revised hypothesis, the proximity of reservoirs of nutrients adjacent to cells may become increasingly important as extracellular matrix deposition limits the availability of nutrients from the external culture bath, leading to increased mechanical and biochemical properties observed in Figure 7.

The inclusion of biocompatible microbubbles appears to be a promising strategy to introduce microporosity to hydrogels in their normally used (hydrated) form. Some of the advantages include preserving the native nanoporosity of the hydrogel as well as the inherent ease of achieving uniform cell seeding associated with hydrogel scaffolds. As microbubble dissolution can be controlled, cell access to fluid-filled micropores can be timed for later culture points when tissue is denser and the benefit of increased porosity may be of greatest significance. The potential importance of creating space for tissue formation later in culture is suggested from our studies demonstrating that controlled enzymatic digestion of glycosaminoglycans from living chondrocyte-seeded agarose constructs leads to constructs with higher collagen content and more functional mechanical properties [48, 49].

5. Conclusions

Microporous agarose scaffolds generated by controlled microbubble dissolution are biocompatible and beneficial, developing a 2-fold increase in engineered cartilage properties (E_Y=492 ± 42 kPa for bubble group vs. 249 ± 49 kPa for bubble-free control group) over a 42 day culture period. This increase was likely due to increased nutrient access to cells in the interior of the scaffold. Our results suggest that microbubbles offer a simple and robust method of modulating mass transfer in cell-seeded hydrogels through mild pressurization, and the methodology may be expanded in the future to include focused ultrasound for improved spatio-temporal control.

Acknowledgments

Funding was provided by NIH R21 EB014382 to C.H., M.B. and E.L. and NIH R01 AR060361 to C.H.

References

1. Ng KW, Wang CC-B, Mauck RL, Kelly TN, Chahine NO, Costa KD, et al. A layered agarose approach tofabricate depth-dependent inhomogeneity in chondrocyte-seeded constructs. J Orthop Res. 2005; 23:134–41. [PubMed: 15607885]
2. Benya PD, Shaffer JD. Dedifferentiated chondrocytes reexpress the differentiated collagen phenotype when cultured in agarose gels. Cell. 1982; 30:215–24. [PubMed: 7127471]
3. Aydelotte, MB.; Schleyerbach, R.; Zeck, BJ.; Kuettner, KE. Articular chondrocytes cultured in agarose gel for study of chondrocytic chondrolysis. In: Kuettner, K., editor. Articular Cartilage Biochemistry. New York: Raven Press; 1986. p. 235-56.
4. Buschmann MD, Gluzband YA, Grodzinsky AJ, Kimura JH, Hunziker EB. Chondrocytes in agarose culture synthesize a mechanically functional extracellular matrix. J Orthop Res. 1992; 10:745–58. [PubMed: 1403287]

5. Lee DA, Bader DL. The development and characterisation of an in vitro system to study strain-induced cell deformation in isolated chondrocytes. In Vitro Cell Dev Biol Anim. 1995; 31:828–35. [PubMed: 8826085]
6. Selmi TA, Neyret P, Verdonk PCM, Barnouin L. Autologous chondrocyte transplantation in combination with an alginate-agarose based hydrogel (Cartipatch). Tech Knee Surg. 2007; 6:253–8.
7. Selmi TA, Verdonk PCM, Chambat P, Dubrana F, Potel JF, Barnouin L, et al. Autologous chondrocyte implantation in a novel alginate-agarose hydrogel: outcome at two years. J Bone Jt Surg. 2008; 90:597–604.
8. Lima EG, Bian L, Ng KW, Mauck RL, Byers BA, Tuan RS, et al. The beneficial effect of delayed compressive loading on tissue-engineered cartilage constructs cultured with TGF-B3. Osteoarthritis Cartilage. 2007; 15:1025–33. [PubMed: 17498976]
9. Bian L, Angione SL, Ng KW, Lima EG, Williams DY, Mao DQ, et al. Influence of decreasing nutrient path length on the development of engineered cartilage. Osteoarthritis Cartilage. 2009; 17:677–85. [PubMed: 19022685]
10. Shi QH, Zhou X, Sun Y. A novel superporous agarose medium for high-speed protein chromatography. Biotechnol Bioeng. 2005; 92:643–51. [PubMed: 16261631]
11. Zhou J, Zhou M, Caruso RA. Agarose template for the fabrication of macroporous metal oxide structures. Langmuir. 2006; 22:3332–6. [PubMed: 16548597]
12. Ho MH, Kuo PY, Hsieh HJ, Hsien TY, Hou LT, Lai JY, et al. Preparation of porous scaffolds by using freeze-extraction and freeze-gelation methods. Biomaterials. 2004; 25:129–38. [PubMed: 14580916]
13. Chen G, Ushida T, Tateishi T. Preparation of poly(L-lactic acid) and poly(DL-lactic-co-glycolic acid) foams by use of ice microparticulates. Biomaterials. 2001; 22:2563–7. [PubMed: 11516089]
14. Feshitan JA, Chen CC, Kwan JJ, Borden MA. Microbubble size isolation by differential centrifugation. J Colloid Interface Sci. 2009; 329:316–24. [PubMed: 18950786]
15. Sirsi S, Feshitan J, Kwan J, Homma S, Borden M. Effect of microbubble size on fundamental mode high frequency ultrasound imaging in mice. Ultrasound in medicine & biology. 2010; 36:935–48. [PubMed: 20447755]
16. Mauck RL, Soltz MA, Wang CC-B, Wong DD, Chao P-HG, Valhmu WB, et al. Functional tissue engineering of articular cartilage through dynamic loading of chondrocyte-seeded agarose gels. J Biomech Eng. 2000; 122:252–60. [PubMed: 10923293]
17. Byers BA, Mauck RL, Chiang I, Tuan RS. Temporal exposure of TGF-B3 under serum-free conditions enhances biomechanical and biochemical maturation of tissue-engineered cartilage. Trans Orthop Res Soc. 2006; 31:43.
18. Park S, Hung CT, Ateshian GA. Mechanical response of bovine articular cartilage under dynamic unconfined compression. Osteoarthritis Cartilage. 2004; 12:65–73. [PubMed: 14697684]
19. Albro MB, Chahine NO, Li R, Yeager K, Hung CT, Ateshian GA. Dynamic loading of deformable porous media can induce active solute transport. J Biomech. 2008; 41:3152–7. [PubMed: 18922531]
20. Chahine NO, Albro MB, Lima EG, Wei VI, Dubois CR, Hung CT, et al. Effect of dynamic loading on the transport of solutes into agarose hydrogels. Biophys J. 2009; 97:968–75. [PubMed: 19686643]
21. Albro MB, Li R, Yeager K, Hung CT, Ateshian GA. Dynamic loading of porous gels and cartilage can induce active solute transport. Tran Orthop Res Soc. 2009:151.
22. Mauck RL, Nicoll SB, Seyhan SL, Ateshian GA, Hung CT. Synergistic effects of growth factors and dynamic loading for cartilage tissue engineering. Tissue Eng. 2003; 9(4):597–611. [PubMed: 13678439]
23. Kelly TA, Ng KW, Ateshian GA, Hung CT. Analysis of radial variations in material properties and matrix composition of chondrocyte-seeded agarose hydrogel constructs. Osteoarthritis Cartilage. 2009; 17:73–82. [PubMed: 18805027]
24. Sirsi SR, Borden MA. Microbubble compositions, properties and biomedical applications. Bubble Science, Engineering and Technology. 2009; 1:3–15. [PubMed: 20574549]
25. Ferrara KW, Borden MA, Zhang H. Lipid-shelled vehicles: engineering for ultrasound molecular imaging and drug delivery. Acc Chem Res. 2009; 42:881–92. [PubMed: 19552457]

26. Ferrara K, Pollard R, Borden M. Ultrasound microbubble contrast agents: Fundamentals and application to gene and drug delivery. Annu Rev Biomed Eng. 2007; 9:415–47. [PubMed: 17651012]
27. Mauck, RL.; Wang, CCB.; Chen, FH.; Lu, HH.; Ateshian, GA.; Hung, CT. Dynamic deformational loading of chondrocyte-seeded agarose hydrogels modulates deposition and structural organization of matrix constituents; 2003 Summer Bioengineering Conference; Key Biscane, FL. 2003;
28. Park JH, Chung BG, Lee WG, Kim J, Brigham MD, Shim J, et al. Microporous cell-laden hydrogels for engineered tissue constructs. Biotechnol Bioeng. 2010; 106:138–48. [PubMed: 20091766]
29. Borden MA, Longo ML. Oxygen permeability of fully condensed lipid monolayers. Journal of Physical Chemistry B. 2004; 108:6009–16.
30. Pu G, Longo ML, Borden MA. Effect of microstructure on molecular oxygen permeability through condensed phospholipid monolayers. J Am Chem Soc. 2005; 127:6524–5. [PubMed: 15869260]
31. Kwan J, Borden M. Microbubble dissolution in a multi-gas environment. Langmuir. 2010; 26:6542–8. [PubMed: 20067292]
32. Borden MA, Pu G, Runner GJ, Longo ML. Surface phase behavior and microstructure of lipid/PEG-emulsifier monolayer-coated microbubbles. Colloids Surf B Biointerfaces. 2004; 35:209–23. [PubMed: 15261034]
33. Epstein-Barash H, Orbey G, Polat BE, Ewoldt RH, Feshitan JA, Langer R, et al. A microcomposite hydrogel for repeated on-demand ultrasound-triggered drug delivery. Biomaterials. 2010; 31:5208–17. [PubMed: 20347484]
34. Seip R, Chin CT, Hall CS, Raju BI, Ghanem A, Tiemann K. Targeted ultrasound-mediated delivery of nanoparticles: on the development of a new HIFU-based therapy and imaging device. IEEE Trans Biomed Eng. 2010; 57:61–70. [PubMed: 19695986]
35. Borden MA, Longo ML. Dissolution behavior of lipid monolayer-coated, air-filled microbubbles: Effect of lipid hydrophobic chain length. Langmuir. 2002; 18:9225–33.
36. Borden MA, Kruse D, Caskey C, Zhao S, Dayton P, Ferrara K. Influence of lipid shell physicochemical properties on ultrasound-induced microbubble destruction. IEEE Transactions on Ultrasonics Ferroelectrics and Frequency Control. 2005; 52:1992–2002.
37. Pu G, Borden MA, Longo ML. Collapse and shedding transitions in binary lipid monolayers coating microbubbles. Langmuir. 2006; 22:2993–9. [PubMed: 16548548]
38. Main ML, Ryan AC, Davis TE, Albano MP, Kusnetzky LL, Hibberd M. Acute Mortality in Hospitalized Patients Undergoing Echocardiography With and Without an Ultrasound Contrast Agent (Multicenter Registry Results in 4,300,966 Consecutive Patients). Am J Cardiol. 2008; 102:1742–6. [PubMed: 19064035]
39. Exuzides A, Main ML, Colby C, Grayburn PA, Feinstein SB, Goldman JH. A Retrospective Comparison of Mortality in Critically Ill Hospitalized Patients Undergoing Echocardiography With and Without an Ultrasound Contrast Agent. Jacc-Cardiovascular Imaging. 3:578–85. [PubMed: 20541713]
40. Wei K, Mulvagh SL, Carson L, Davidoff R, Gabriel R, Grimm RA, et al. The Safety of Definity and Optison for Ultrasound Image Enhancement: A Retrospective Analysis of 78,383 Administered Contrast Doses. J Am Soc Echocardiogr. 2008; 21:1202–6. [PubMed: 18848430]
41. Borden MA, Zhang H, Gillies RJ, Dayton PA, Ferrara KW. A Stimulus-Responsive Contrast Agent for Ultrasound Molecular Imaging. Biomaterials. 2008; 29:597–606. [PubMed: 17977595]
42. Chen CC, Borden MA. The role of poly(ethylene glycol) brush architecture in complement activation on targeted microbubble surfaces. Biomaterials. 2011; 32:6579–87. [PubMed: 21683439]
43. De Temmerman ML, Dewitte H, Vandenbroucke RE, Lucas B, Libert C, Demeester J, et al. mRNA-Lipoplex loaded microbubble contrast agents for ultrasound-assisted transfection of dendritic cells. Biomaterials. 2011; 32:9128–35. [PubMed: 21868088]
44. Feshitan JA, Vlachos F, Sirsi SR, Konofagou EE, Borden MA. Theranostic Gd(III)-lipid microbubbles for MRI-guided focused ultrasound surgery. Biomaterials. 2012; 33:247–55. [PubMed: 21993236]

45. Ting CY, Fan CH, Liu HL, Huang CY, Hsieh HY, Yen TC, et al. Concurrent blood-brain barrier opening and local drug delivery using drug-carrying microbubbles and focused ultrasound for brain glioma treatment. Biomaterials. 2012; 33:704–12. [PubMed: 22019122]

46. Nair A, Thevenot P, Dey J, Shen J, Sun MW, Yang J, et al. Novel polymeric scaffolds using protein microbubbles as porogen and growth factor carriers. Tissue Eng Part C Methods. 2010; 16:23–32. [PubMed: 19327002]

47. Lima, EG.; Ye, M.; Samojlik, SK.; Stoker, A.; Sirsi, SR.; Borden, MA., et al. Platen-Less Deformational Loading of Cell-Seeded Scaffolds for Cartilage Mechanobiology and Tissue Engineering; Orthopaedic Research Society Annual Meeting; San Francisco. 2012;

48. Ng, KW.; Ateshian, GA.; Hung, CT. Trans Orthop Res Soc. 2008. Layered hydrogel cartilage constructs using zonal chondrocytes; p. 33in press

49. Bian L, Crivello KM, Ng KW, Xu D, Williams DY, Ateshian GA, et al. Influence of Temporary Chondroitinase ABC-Induced Glycosaminoglycan Suppression on Maturation of Tissue-Engineered Cartilage. Tissue Eng Part A. 2009; 15:2065–72. [PubMed: 19196151]

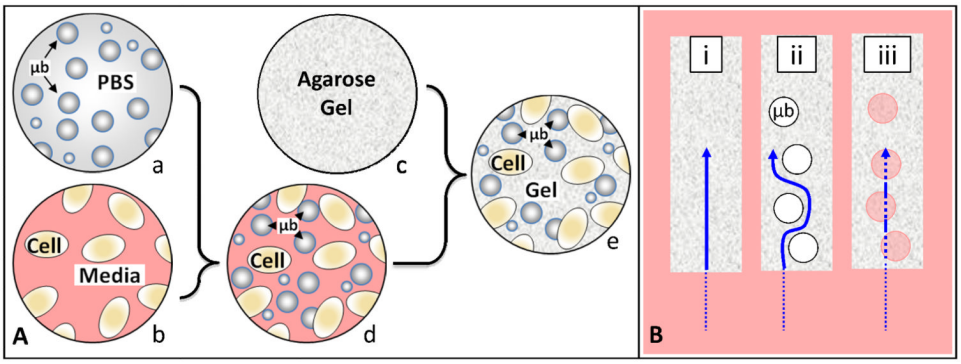

Figure 1.

A) Schematic of the steps entailed in assembling microbubble-infused agarose hydrogel constructs where; (a) a known concentration of microbubbles suspended in Phosphate Buffered Saline is combined with (b) cells suspended in media to create (c) a microbubble/cell slurry, which is then combined with (d) molten agarose at 37°C to create (e) the final cell-seeded microbubble hydrogel constructs. **B)** Anticipated solute diffusion pathway (arrow) through bubble-free hydrogels (i), and through microbubble-infused hydrogels before (ii) and after (iii) the gas is purged from the interior of the microbubbles.

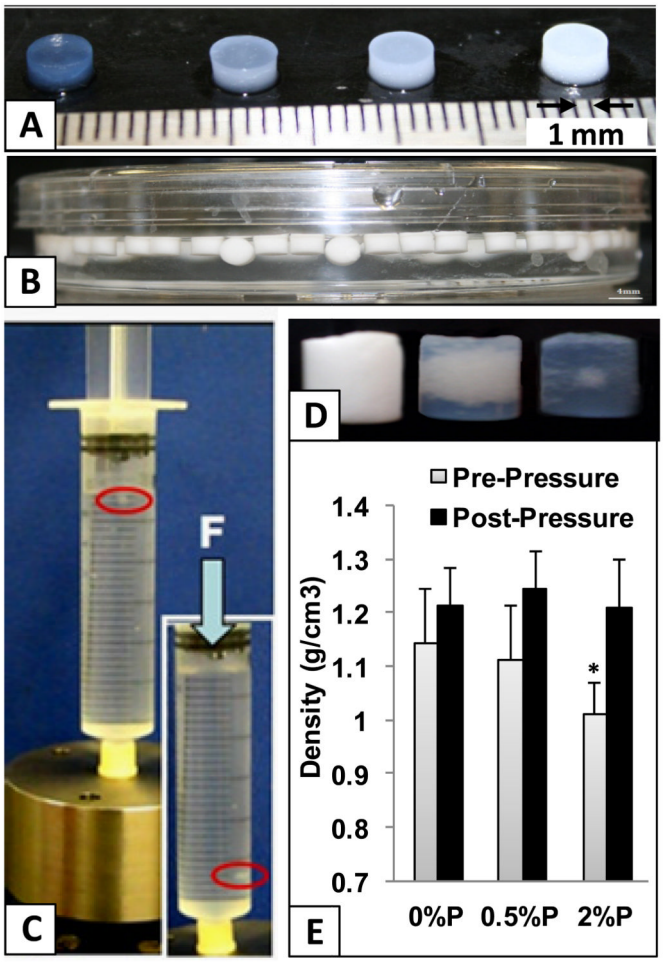

Figure 2.

A) Hydrogel constructs infused with gas-filled microbubbles show concentration-dependent opacity. B) Side view of a petri dish filled with PBS; At high concentrations microbubble constructs float, but C) sink when subjected to hydrostatic pressure (noted by red ellipse). D) View of whole-construct becoming less opaque with pressure-induced microbubble dissolution over time (0,1,3 hours at, 270 kPa). E) Density measurements pre/post-pressurization. *=$p<0.01$ vs. other groups (n=12)

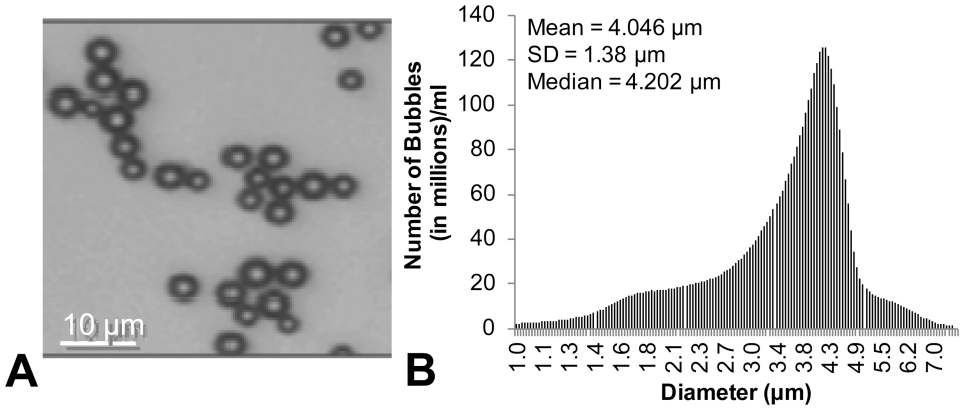

Figure 3.
A) Microscopic view of microbubbles in PBS. B) Size distribution of microbubbles prior to embedding within agarose.

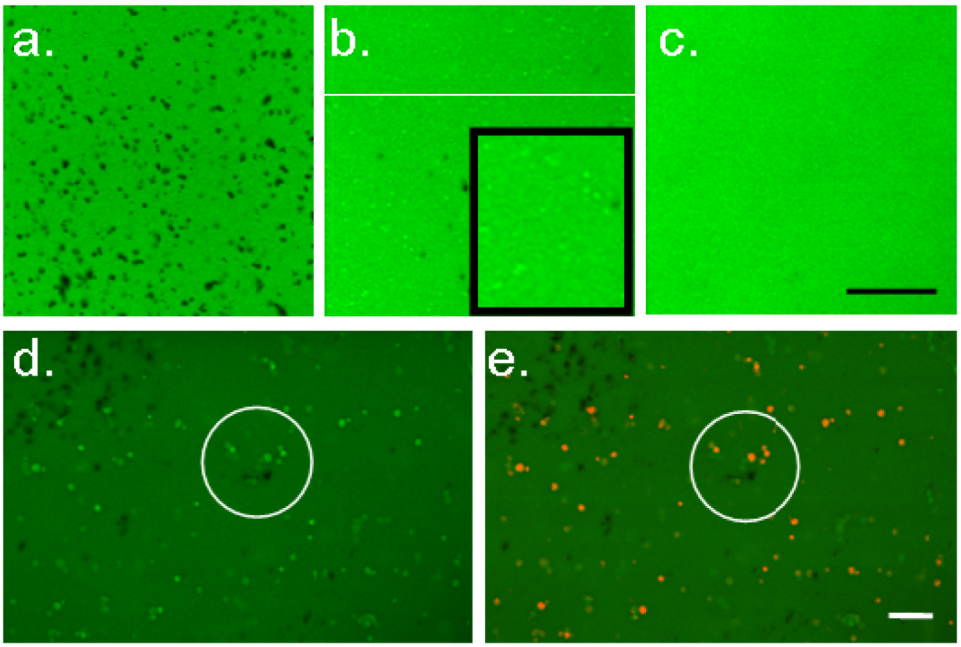

Figure 4.

Top, 2% v/v microbubble constructs saturated in media containing FITC-conjugated dextran (a.) on day 1 with microbubbles appearing black and (b.) on day 8 with microbubbles appearing as brighter green regions (pools of FITC-conjugated dextran). Inset shows digital zoom, highlighting bright zones (c.) Control constructs on day 8. *Bottom.* Microbubble constructs stained with Dil on day 8 (same view): (d.) Dil unexcited and (e.) Dil excited (red), demonstrating co-localization of dextran pools and lipid remnants. Scale bars indicate 100 μm.

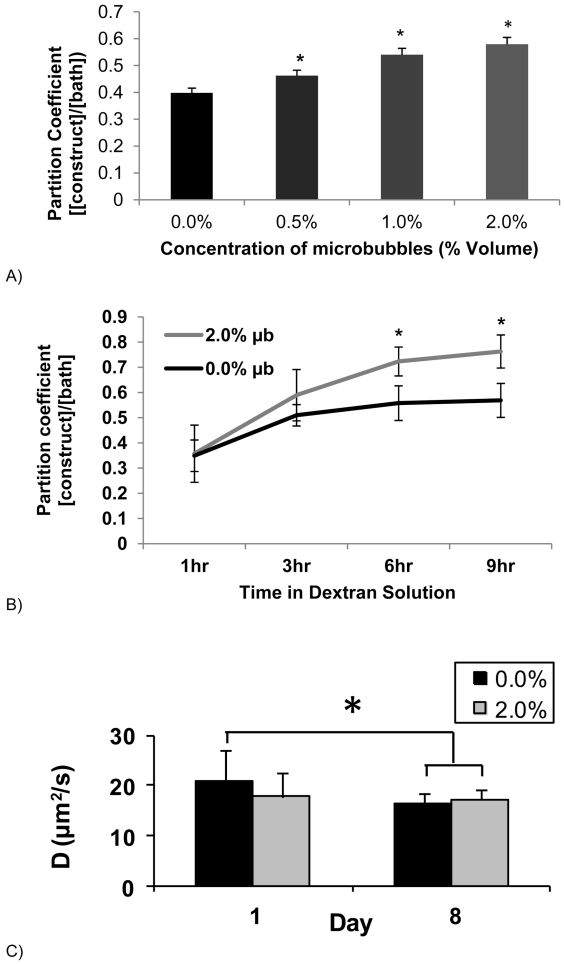

Figure 5.

A) The Absorption coefficient ([dextran in constructs]/[dextran in bathing solution]) of microbubble constructs at 4 different microbubble concentrations after a 3 hour soak in 70 kD dextran (0.5mg/mL). *=<0.05 against other groups (n=9). B) Absorption coefficient for a single concentration of microbubbles (2.0%) over time. *=<0.01 against control group (n=4-6/group and time point). C) Diffusion coefficients ($\mu m^2/s$) localized within constructs using FRAP analysis comparing control and 2.0% microbubble constructs on days 1 and 8. Asterisk represents significance, * $p \leq 0.05$ (n=6/group and time point).

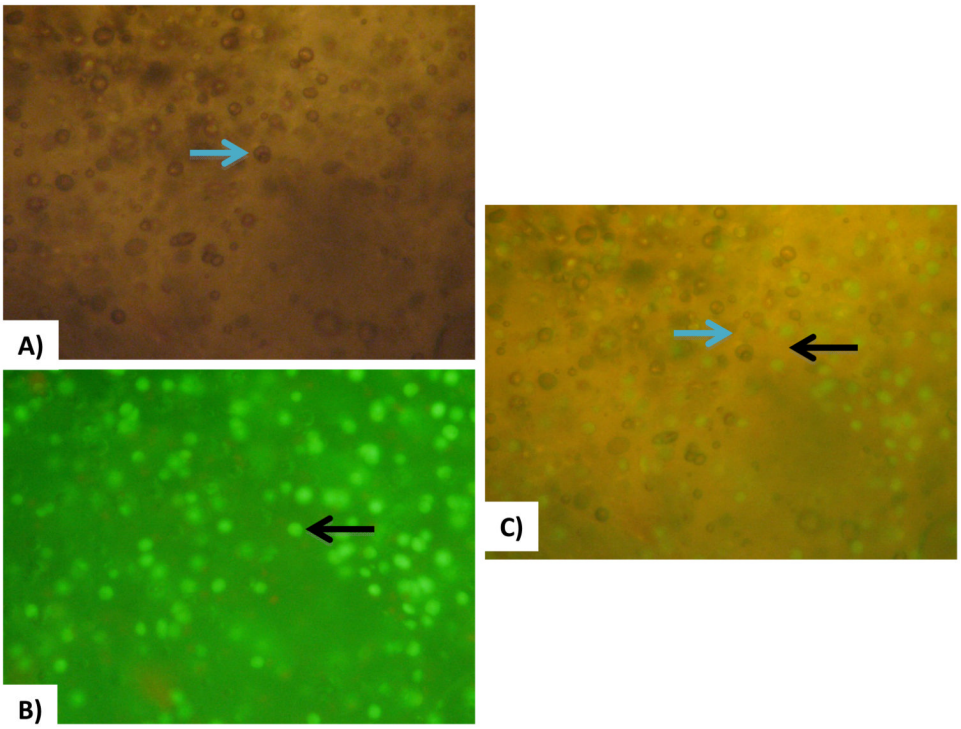

Figure 6.

A) Bright field microscopy of bubble-embedded cellular constructs (blue arrow directed at bubble). B) Fluorescence microscopy of bubble-embedded cellular constructs; Calcein AM dye causes the living cells to fluoresce green (black arrow directed at cell). C) Combination of both lighting systems for visualization of cells and bubble coexistence (blue arrow directed at bubble and black bubble directed at cell).

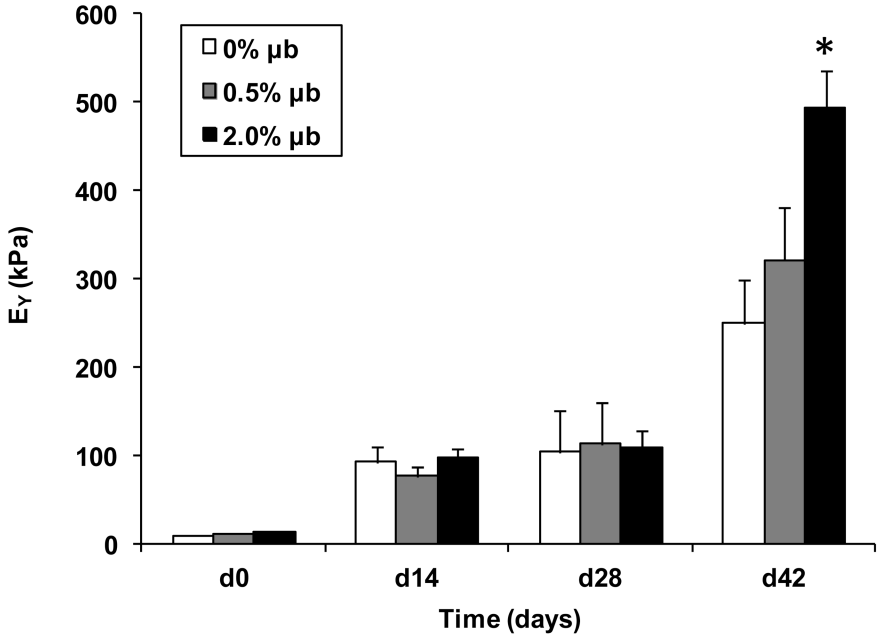

Day 42	G*1Hz(MPa)	GAG/DNA	Col/DNA
0.0% µb	3.04±0.87	29.37±6.06	7.95±1.60
0.5% µb	3.56±0.83	38.52±8.84	8.19±.026
2.0% µb	3.76±0.82*	47.51±13.01*	11.90±2.90*

Figure 7.
Equilibrium Young's modulus and dynamic modulus of constructs throughout culture time. Biochemical properties reported for D42 final values. *$p<0.01$ vs. 0.0% µb control (n=9-11/group and time point).